J. Fluid Mech. (1993), *vol.* 254, *pp.* 501–527

Bjerknes forces between two bubbles. Part 2. Response to an oscillatory pressure field

By NIKOLAOS A. PELEKASIS AND JOHN A. TSAMOPOULOS

Department of Chemical Engineering, State University of New York at Buffalo, Buffalo, NY 14260, USA

(Received 11 November 1991 and in revised form 16 March 1993)

The motion of two gas bubbles in response to an oscillatory disturbance in the ambient pressure is studied. It is shown that the relative motion of bubbles of unequal size depends on the frequency of the disturbance. If this frequency is between the two natural frequencies for volume oscillations of the individual bubbles, the two bubbles are seen to move away from each other; otherwise attractive forces prevail. Bubbles of equal size can only attract each other, irrespective of the oscillation frequency. When the Bond number, *Bo* (based on the average acceleration) lies above a critical region, spherical-cap shapes appear with deformation confined on the side of the bubbles facing away from the direction of acceleration. For *Bo* below the critical region shape oscillations spanning the entire bubble surface take place, as a result of subharmonic resonance. The presence of the oscillatory acoustic field adds one more frequency to the system and increases the possibilities for resonance. However, only subharmonic resonance is observed because it occurs on a faster timescale, $O(1/\epsilon)$, where ϵ is the disturbance amplitude. Furthermore, among the different possible periodic variations of the volume of each bubble, the one with the smaller period determines which Legendre mode will be excited through subharmonic resonance. Spherical-cap shapes also occur on a timescale $O(1/\epsilon)$. When the bubbles are driven below resonance and for quite large amplitudes of the acoustic pressure, $\epsilon \approx 0.8$, a subharmonic signal at half the natural frequency of volume oscillations is obtained. This signal is primarily associated with the zeroth mode and corresponds to volume expansion followed by rapid collapse of the bubbles, a behaviour well documented in acoustic cavitation experiments.

1. Introduction

It is very well documented in the field of acoustic cavitation that pressure changes determine the dynamic, and eventually destructive, behaviour of bubbles in high-speed flows. In order to study the effect of pressure, it is common practice in experimental studies of cavitation to set the host fluid along with the trapped bubbles in pulsation using a sound field. In the pioneering work of Kornfeld & Suvorov (1944), a vibrating cylinder was used for the generation of air bubbles in water which were then observed as they oscillated and in some cases translated in the fluid at a high speed. The accelerating motion of the bubbles was attributed by the above investigators to the well-known 'Bjerknes effect'. According to Bjerknes (1906, 1909) two bubbles oscillating in a sound field will attract or repel each other depending on whether they oscillate in or out of phase, respectively. In the same study it was observed that increasing the amplitude of vibrations intensifies the accelerating motion of the bubbles

until at some point they are seen to move violently in a 'zig-zag' pattern. These bubbles have been called 'dancing bubbles'. For relatively small amplitudes however, the bubbles were observed to perform complicated vibrations accompanied by non-spherical shapes, and eventually to coalesce or disintegrate.

The wealth of hydrodynamic effects involved in acoustic cavitation attracted several investigators to the field. A brief summary of the literature related to the Bjerknes effect is given in Part 1 of this work (Pelekasis & Tsamopoulos 1993), where the effect of a step change in the static pressure is examined. Only the additional literature relevant to the present problem will be discussed below. Eller & Crum (1970) studied the possibility of shape oscillations for a single bubble already undergoing radial oscillations. The bubble was trapped in a standing wave which provided the pressure gradient needed for balancing gravity. The motion was induced by an acoustic pressure field which oscillated in time, and was imposed on top of the original standing wave. They conducted an asymptotic analysis, valid only for small values of the amplitude of the acoustic sound wave, to obtain the amplitude thresholds for the onset of shape oscillations with frequency one half of the driving frequency, of the acoustic pressure. Comparing the calculated values with experimentally obtained results for the onset of the erratic motion of bubbles, they concluded that the latter effect is caused by the parametric excitation of shape oscillations. This mechanism was originally proposed by Benjamin & Strasberg (1958).

More recently Hall & Seminara (1980) carried out a more systematic nonlinear stability analysis of the same problem posed by Eller & Crum. Under the assumption of axisymmetric and potential flow, the basic oscillatory motion in the radial direction was found to bifurcate into a non-spherosymmetric motion. This motion was periodic on the fast timescale imposed by the acoustic excitation and its amplitude was slowly modulated on the timescale associated with the linear growth rate of specific axisymmetric disturbances. Perturbation theory gave rise to an equation of the Mathieu type (Bender & Orszag 1978), which was solved for the linear growth rates and the thresholds for stability of non-spherical shape oscillations. The effect of the natural frequency for radial oscillations was not examined. However, it is shown in the present study that it is primarily this frequency that interacts with the frequencies of the higher modes, although the scaling arguments introduced by Hall & Seminara are still valid.

The coupling of the effects of bubble acceleration and shape oscillations is examined in Part 1. There, a step change in pressure generates 'Bjerknes forces' between the two bubbles, which induce an accelerating motion whose intensity is measured by the Bond number, $Bo = (\langle g^* \rangle R^{*2}\rho)/\sigma$; where $\langle g^* \rangle$ is the average acceleration of each centre of mass, R^* is the bubble radius, σ is the interfacial tension and ρ is the fluid density. For bubbles of equal size Bo is identical to the average dimensionless acceleration. For Bo sufficiently large, acceleration overwhelms surface tension to produce spherical-cap shapes that are deformed only on the side facing away from the direction of acceleration. Spherical-cap shapes were first observed and explained in steadily rising bubbles of sufficiently large volume by Davies & Taylor (1950). When Bo is below a critical range of values, bubbles with globally deformed shapes arise. Such shapes were repeatedly observed by Kornfeld & Suvorov in their acoustic cavitation experiments. They are dominated by Legendre modes, oscillating at a frequency half that of volume oscillations. This is a result of subharmonic excitation of certain Legendre components of the shape by the pulsating motion of the two bubbles. Both effects occur when time becomes $O(1/\epsilon)$, where ϵ is a measure of the amplitude of the change in the static pressure. The above scaling for time was predicted by Hall & Seminara for

subharmonic resonance and was also established numerically in Part 1 for spherical-cap shapes.

Bubble acceleration and shape oscillations are secondary effects, since any disturbance in the far-field pressure primarily induces radial pulsations of the bubbles. In fact, early research in cavitation was targeted towards understanding the dynamics of a single bubble undergoing radial oscillations. An extensive account of the early literature in the field is given by Plesset & Prosperetti (1977) in a review paper. Most notably Flynn (1964) carried out a number of numerical simulations of the radial oscillations of a single bubble set in motion by an acoustic sound field. His results demonstrated the complexity of possible responses. In particular he was able to capture the explosive behaviour of the bubble during cavitation, consisting of volume growth followed by violent collapse to small values of the radius. Lauterborn (1976) and Lauterborn & Cramer (1981) conducted an extensive numerical investigation of the same problem. They were thus able to recover a very complicated pattern of resonances between the forcing frequency, ω_f, and the natural frequency of the bubble for linear oscillations, ω_0, which dominate the steady-state response for sufficiently large amplitudes of the acoustic pressure variation.

In the same context as the above studies, Esche (1952) reported a subharmonic component, i.e. a signal at half the forcing frequency, in the spectrum of a liquid undergoing acoustic cavitation. This experimental result gave rise to the hypothesis that subharmonically oscillating bubbles evolve into transient cavities that eventually collapse and breakup and thus produce the severe effects associated with acoustic cavitation. Later Neppiras (1969) provided experimental evidence that a subharmonic signal may be produced by forced oscillations of bubbles whose radial resonance frequencies are submultiples of the forcing frequency, ω_f. Furthermore, in certain cases he observed that when the concentration of bubbles with sizes corresponding to the frequencies prescribed above was low, the subharmonic signal was very weak. However, his results were not conclusive and he had to conjecture the existence of some additional mechanism unrelated to resonant bubbles, that contributes to the strong subharmonic signals.

In the present study the motion of two initially static and spherical bubbles induced by an acoustic field is examined. When gravitational effects are small there is no need for a standing wave to trap the bubbles and the motion can be simply induced by perturbing the static pressure at infinity, P_s. The perturbation is periodic in time with frequency ω_f, and amplitude ϵP_s. In §2 a brief account is given of the specific features of the problem treated here, whereas the details of the problem formulation and numerical solution are given in Part 1.

The presence of the forcing frequency, ω_f, introduces one additional important timescale into the problem, besides the ones associated with the natural frequency of volume oscillations for each bubble. The latter alone govern the primary oscillatory motion in the case of a step change in pressure. Therefore, the possibilities for resonance and the number of competing effects increase. Moreover, in the case of bubbles with unequal size, ω_f induces oscillations that result in attraction or repulsion depending on the specific phase difference. In §3 a summary of the results obtained in Part 1 that are relevant to the present study, is given. Next, in §4 the long-time behaviour of two equal bubbles is presented in response to an oscillatory pressure field and the dominant effects are identified as a function of the problem parameters. In several instances the response can be classified as in cases with a step change in pressure. For large values of the amplitude, ϵ, however, radial oscillations become the dominant effect and a signal at half the natural frequency is obtained irrespective of the

magnitude of the forcing frequency. The response of two unequal bubbles to a step change in pressure is presented in §5. The behaviour of each bubble is determined by its individual Bond number. When a periodically varying pressure field is applied the two bubbles are seen to repel or attract each other depending on whether the forcing frequency is within the interval defined by their natural frequencies, or outside it, §6. Finally, in §7 the results presented here are discussed in the context of previous investigations and future directions are suggested.

2. Problem statement

The flow field examined here is similar to that in Part 1, with the exception of the initial disturbance. More specifically, the motion of two inertialess bubbles is studied. Their shape is initially spherical with dimensionless radii $R_1 = 1$ and $R_2 = R \leqslant 1$, for the left and right bubbles, respectively. The pressure inside the gas bubbles changes adiabatically and instantaneously follows the dynamics of the liquid at the gas–liquid interface. The centres of mass of each bubble are initially located at a dimensionless distance apart $D > 1+R$. Lengths are made dimensionless through the radius of the left bubble, whereas surface tension and liquid density are used for making pressure, P, velocity potential, Φ, and time, t, dimensionless. The liquid surrounding the two cavities is taken to be inviscid and the flow in it incompressible and irrotational.

The two gas–liquid interfaces are treated as free surfaces and are calculated along with the velocity potential and normal velocity at both interfaces in every time step. To this end, a hybridization of the boundary element method and the finite element method (or collocation) is used as discussed in Pelekasis, Tsamopoulos & Manolis (1991, 1992). Gravitational effects are neglected. When $t < 0$ the static pressure everywhere in the liquid, P_s, is uniform. At time, $t = 0$, an acoustic pressure field is applied at infinity, where the total dimensionless pressure is prescribed as

$$P_\infty = P_s(1+\epsilon\cos\omega_f t), \quad t \geqslant 0, \tag{2.1}$$

with ϵ being the measure of the amplitude of the disturbance and ω_f the forcing frequency. Summarizing, the parameters involved in the analysis are the ratio of the two radii R, the initial distance between the two centres of mass D, the static pressure P_s, and the amplitude and frequency of the acoustic sound field, ϵ and ω_f.

The problem formulation through the Eulerian or the mixed Lagrangian–Eulerian approach is described in detail in Part 1. Owing to the oscillatory pressure change at infinity the total energy of the system, as given by (2.27) in Part 1, does not remain constant. Instead, it oscillates in time with the period of the acoustic pressure field. It can be shown that the variation of the total energy, E, with time is prescribed by the following relation:

$$\mathrm{d}E/\mathrm{d}t = -2\omega_f \epsilon P_s(V_1 + V_2)\sin\omega_f t, \tag{2.2}$$

where V_1 and V_2 denote the instantaneous volumes of the left and right bubbles, respectively. The above equation can be obtained by using

$$\int_V \frac{\partial \Phi}{\partial t}\nabla^2\Phi \,\mathrm{d}V = 0 \tag{2.3}$$

and then proceeding with integration by parts and employing the kinematic and dynamic boundary conditions. The amplitude of the energy oscillations does not necessarily remain constant and as ω_f approaches the natural frequency for volume oscillations, ω_0, it is seen to increase. Any slight deviation from (2.2) can serve as an

accuracy check for the computations. This becomes more convenient when (2.2) is integrated as follows:

$$E(t) = E(t=0) - \int_0^t 2\omega_f \epsilon P_s (V_1 + V_2) \sin \omega_f t \, \mathrm{d}t. \tag{2.4}$$

The numerical solution of the system of equations is also described in Part 1 for both the Eulerian and mixed formulation. However, the mixed formulation is used throughout the present study, in spite of its lower accuracy at early times (see Part 1), since it can capture the more complicated shapes that arise at later times. For most computed cases the basic timescale is that of the natural volume oscillations. In general the step for time integration is selected in such a way as to allow for at least 100 time steps per period of the natural volume oscillations.

When $P_s = 666.66$, $R = 1$, $D = 4$ and $\epsilon = 0.2$ the period of natural volume oscillations was found in Part 1 to be 0.082. In this case, a time step of $\Delta t = 0.0005$ allows for 164 time steps per period. This time step is small enough to be used even in the few cases where the forcing frequency is larger than the natural frequency of volume oscillations. For the same reason a time step of 0.002 is used when $P_s = 50$. Normally 41 nodal points are used for each interface. In several cases and towards the late stages of motion, shape deformations become very large and evolve on a very small timescale. In order to accurately capture the motion under such conditions the time step is halved and the number of nodal points is doubled to 81. Finally the trapezoidal rule is used for integrating (2.4). For all the cases examined the two sides of (2.4) are in agreement to within at least the first two significant digits.

3. General characteristics

As already pointed out, one very interesting feature of the physical system studied here is that it allows for the coupling of several very important effects in the area of acoustic cavitation. Namely, the primary effect of radial oscillations can, under certain conditions, lead to non-spherical shape oscillations through resonance with specific Legendre modes (Hall & Seminara 1980). In addition, the nonlinear interaction between the two bubbles induces an accelerating motion of their two centres of mass along their common axis of symmetry. If this induced acceleration is large enough spherical-cap shapes arise.

In the following, the modes corresponding to natural volume or radial oscillations of each bubble (zeroth mode) will be referred to as breathing modes. The rest of the eigenmodes and bubble shapes can be represented by the Legendre modes obtained through decomposition of the shape in a spherical coordinate system based on the instantaneous centre of mass of each bubble. The variation with time of the resulting coefficients, c_i, will be plotted occasionally in order to demonstrate different types of mode coupling.

For a step change in pressure at infinity, the frequency of volume oscillations is approximately that predicted by linear theory and is called the natural frequency; see Part 1 for its calculation. Furthermore, it varies with $P_s^{\frac{1}{2}}$ for large enough values of P_s and D, and with $R_i^{-\frac{3}{2}}$ for relatively large values of R_i and D. For bubbles of equal size there are two natural frequencies, corresponding to symmetric and antisymmetric oscillations, respectively. The frequency of the symmetric mode is found to decrease with decreasing distance D, whereas the opposite is true for the antisymmetric mode. On the other hand the eigenfrequencies of all the higher modes depend very weakly on both D and P_s, but they also vary as $R_i^{-\frac{3}{2}}$ with the bubble radius. Even when the two

bubbles are not equal in size two sets of eigenfrequencies exist, for each set of values of D, R and P_s, each one affecting primarily one of the two bubbles. The corresponding eigenvectors are dominated by a specific Legendre mode; see tables 1 and 2 and the linear analysis in Part 1 for more details. In particular, as was shown in Part 1, the numerical values of the eigenfrequencies of all the modes, except for the zeroth mode, can be well approximated by the well-known formula

$$\omega^2 = \frac{(n^2-1)(n+2)}{R_i^3}, \quad n > 1, \tag{3.1}$$

which becomes exact as $D \to \infty$ (isolated bubbles), see Lamb (1932). These values are repeatedly used in the next sections. In the same limit, $D \to \infty$, the frequency of the radial oscillation for each bubble is given by

$$T_{0,\infty} = \frac{2\pi}{\omega_{0,\infty}} = \frac{2\pi}{[6(P_s+1/R)\gamma/R^2 - 2/R^3]^{\frac{1}{2}}}. \tag{3.2}$$

A systematic analysis of several new possibilities, when $\omega_f \neq 0$, follows.

4. Bubbles of equal size in an oscillatory pressure field

The forcing frequency can be chosen in such a way as to induce subharmonic or harmonic resonance with the Legendre modes describing the shape of the bubbles. At the same time, there is always the possibility of resonance between the breathing mode of the two bubbles and the Legendre modes. In fact, it is safe to assume that given any periodic motion performed by the volume of either one of the two bubbles, there will always be one or more modes in the linear spectrum that will be in harmonic or subharmonic resonance with the volume oscillations. Alternatively, in a suspension of bubbles there will always exist some whose size will permit resonance.

When the bubbles are of unequal size, $R \neq 1$, the two sets of eigenvalues, each corresponding to one of the two bubbles, are equally important in the description of the motion. In order to avoid the complications introduced by the additional timescales we choose to study bubbles of equal size first. Consequently, when the bubbles are initially at equilibrium in the host fluid and a spatially uniform disturbance in pressure is applied, only the in-phase mode may be excited in both bubbles. This reduces the number of timescales involved in the motion by one set and simplifies the study on the coupling between the effects of resonance and acceleration for varying parameter values.

4.1. *Bubbles at distance $D = 8$ and initial pressure $P_s = 666.66$*

It was found in Part 1 (figure 10) that when $\epsilon = 0.2$ shape oscillations arise on the outer surface of both bubbles at $t \approx 1.4$, as a result of subharmonic resonance between the breathing mode and certain high modes, P_8, P_9 and P_{10}. When ϵ increases to 0.4 (figure 12 in Part 1) the stronger translation of both bubbles confines deformation to the side of the bubbles away from the direction of acceleration while the rest of the shape resembles that of a sphere. Both effects occur when time becomes $O(1/\epsilon)$ and the transition between these two different behaviours is determined by the average acceleration, $\langle g \rangle$, which is proportional to ϵ^2. In particular, spherical-cap shapes appear when $\langle g \rangle$ exceeds a critical range of values. For example, when $P_s = 666.66$, i.e. $P_s^* = 1$ atm for bubbles with $R_i^* = 1$ mm in water, this critical range was found to be $1.0 \leqslant Bo \leqslant 1.5$. This was the recurring theme in Part 1 and it is seen in the following that it persists in the present study with the exception of very large amplitudes.

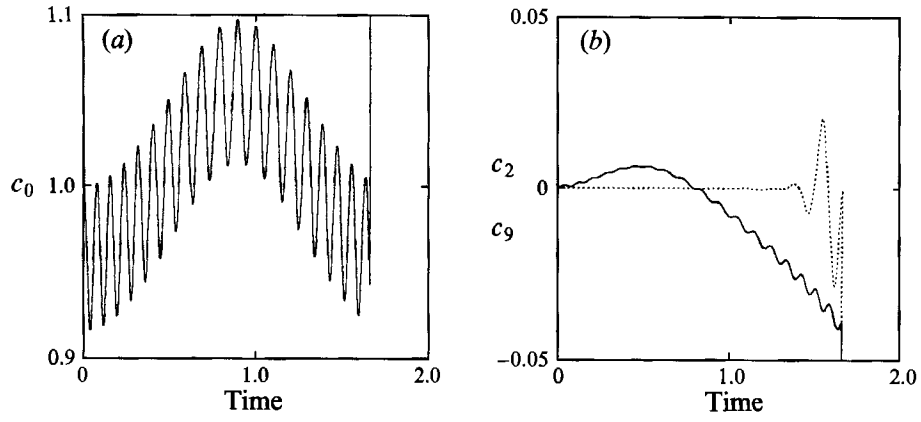

FIGURE 1. Variation with time of selected Legendre coefficients: (*a*) c_0, (*b*) ——, c_2; ..., c_9, of the shape of the left bubble; $R = 1$, $D = 8$, $P_a = 666.66$, $\epsilon = 0.2$ and $\omega_f = 3.5$. The right bubble behaves in the same way owing to symmetry.

Turning now to a disturbance in pressure that oscillates with $\omega_f = 3.5$ and $\epsilon = 0.2$ it is found that shape oscillations occur a little later, at time $t \approx 1.6$. Until then, all modes shown in figure 1 oscillate with the breathing-mode frequency, which is approximately $\omega_0 = 70$. This is detectable in the second mode which also grows slowly, whereas it cannot be seen as clearly in the ninth mode owing to the scale used in plotting their amplitudes. The external disturbance has not even completed a period ($T_f = 2\pi/\omega_f \approx 1.8$) when calculations break down at $t \approx 1.7$ due to exponential growth of all the modes. Therefore, the latter effect is caused by resonance with the zeroth mode and not the forcing. Indeed, at $t \approx 1.6$ the coefficients P_8, P_9 and P_{10} become dominant in the bubble shape. This is also evident from the number of lumps appearing on the outer surface of the two bubbles. These shapes are given in Pelekasis (1991) and they resemble those in figure 10 of Part 1 except that the overall amplitude of deformation is smaller. The acceleration is averaged over each period of the breathing mode and it is found that for both bubbles it follows the oscillations of the pressure field, table 1. At the same time the amplitude of volume oscillations is changing with time and is modulated by the forcing frequency (compare figure 1 (*a*) here with figure 11 (*a*) in Part 1). The maximum, minimum and mean values of the average acceleration are 0.69, 0.26 and 0.47 respectively. The latter is less than the average acceleration induced when $\omega_f = 0$ and all are below the critical range of *Bo*.

Equations (3.1) and (3.2) show that the approximate eigenfrequencies of the modes P_8–P_{10} are about one half the frequency of ω_0. The presence of a second bubble and of nonlinearities leads to subharmonic resonance with at least three Legendre modes as opposed to just one that could have been anticipated theoretically. The delay in the appearance of subharmonic resonance, as compared with the case of a step change in pressure, is because, on average, less energy is now available in the system. It should also be noted that the frequency of the acoustic pressure is very close to the linear frequency of P_2. However, the slow variation of P_2 cannot be attributed to its harmonic resonance with the forcing, but rather to its forced oscillation with its eigenfrequency. This should be expected since subharmonic resonance becomes evident when $t = O(1/\epsilon)$, whereas harmonic resonance occurs when $t = O(1/\epsilon^2)$ (Hall & Seminara 1980). Increasing ω_f to 7 again induces shape oscillations dominated by P_8, P_9 and P_{10} due to subharmonic resonance with the zeroth mode. It is also worth noting that even

	$\omega_f = 3.5$		$\omega_f = 34.5$	
Period	Time interval	$\langle g \rangle$	Time interval	$\langle g \rangle$
1	0.021–0.1	0.46	0.019–0.134	1.94
2	0.1–0.179	0.47	0.134–0.21	0.66
3	0.179–0.26	0.41	0.21–0.324	3.07
4	0.26–0.343	0.39	0.324–0.4	1.16
5	0.343–0.43	0.33	0.4–0.512	5.04
6	0.43–0.521	0.27	0.512–0.589	1.62
7	0.521–0.616	0.26	0.589–0.698	8.27
8	0.616–0.716	0.27		
9	0.716–0.82	0.31		
10	0.82–0.926	0.37		
11	0.926–1.031	0.47		
12	1.031–1.134	0.53		
13	1.134–1.232	0.61		
14	1.232–1.325	0.67		
15	1.325–1.414	0.69		
16	1.414–1.499	0.68		

TABLE 1. Variation of the average acceleration, $\langle g \rangle$, of the two centres of mass over a number of periods of the breathing mode; $R = 1$, $D = 8$, $\epsilon = 0.2$, $P_s = 666.66$. The time intervals defining the periods correspond to zeros in the oscillations of the acceleration.

subharmonic resonance between the increased frequency of the external oscillation and P_2 does not have the time to evolve, although it could have been anticipated by the relative magnitude of their frequencies.

Another possibility for resonance, superharmonic this time, lies in the interaction between the forcing pressure and the breathing mode. For this reason, the response of the system is computed with ϵ set to 0.2 and ω_f set to 34.5, which is roughly half the frequency of the breathing mode, $\omega_0 = 70$. As a result, the amplitude of the volume oscillations increases very rapidly. This can be monitored through the oscillations of c_0 which exhibit both frequencies, see figure 2. Consequently the acceleration of both bubbles increases and the shape deformation is confined to the rear side of the two bubbles only, although ϵ/D is relatively small, see figure 3. Energy from the zeroth mode is quickly transferred to all the other modes, which grow more than in the previous case and before subharmonic resonance of P_9 and P_{10} can be clearly detected; see Pelekasis (1991). The average acceleration again follows the oscillations of the acoustic field, see table 1, and towards the end of computations becomes significantly larger than 1.5, thus giving rise to spherical-cap shapes.

4.2. *Bubbles at initial pressure* $P_s = 50$

Quite often in cavitation experiments taking place in a venturi for instance, the datum pressure is below the atmospheric level. Then new interactions become possible. For example, the frequency of the breathing mode may approach the linear frequencies of the lower Legendre modes. When the static pressure is set to 50, i.e. $P_s^* = 0.075$ atm for $R_i^* = 1$ mm in water and $D = 4$, linear theory predicts that $\omega_0 = 18.5$. In this case and for a step change in the static pressure the critical *Bo* is found to be between 0.55 and 1.2, corresponding to $\epsilon = 0.4$ and 0.6 respectively. This range is below the critical range obtained when $P_s = 666.66$, which was 1.0–1.5, since the static pressure has been decreased, see Part 1. As *Bo* increases beyond 1.2 spherical-cap shapes appear, whereas for smaller values subharmonic resonance occurs between the breathing mode and the

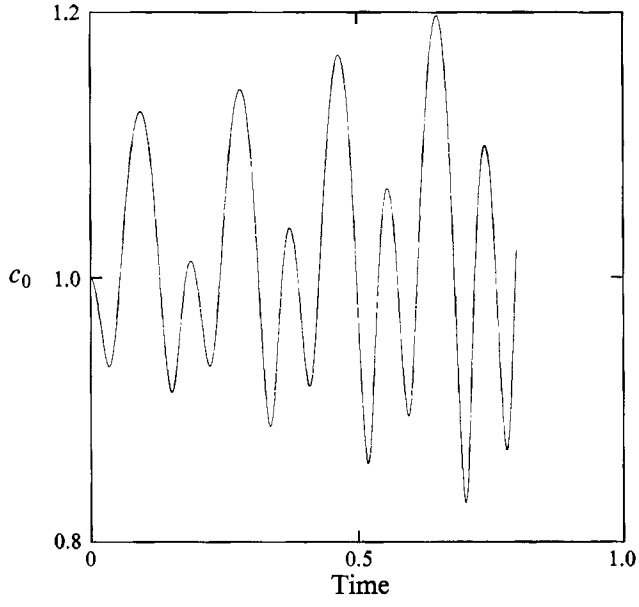

FIGURE 2. Variation with time of the zeroth Legendre coefficient, c_0, of the shape of the left bubble when the forcing frequency is half the frequency of the breathing mode; $R = 1$, $D = 8$, $P_s = 666.66$, $\epsilon = 0.2$ and $\omega_f = 34.5$. The right bubble behaves in the same way owing to symmetry.

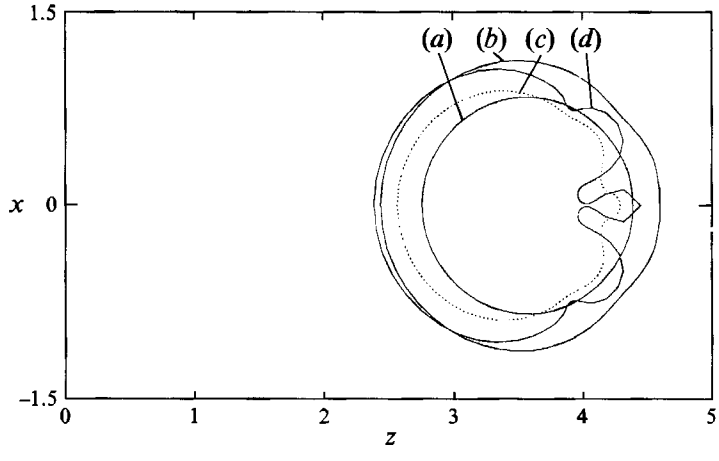

FIGURE 3. Bubble shapes, obtained up to breakdown of computations with $R = 1$, $D = 8$, $P_s = 666.66$, $\epsilon = 0.2$ and $\omega_f = 34.5$, at (*a*) $t = 0.70$, (*b*) $t = 0.74$, (*c*) $t = 0.78$ and (*d*) $t = 0.80$.

Legendre modes c_4, c_5 and c_6. The dependence of the time at which instabilities arise and of the Bond number on ϵ remains the same as when $P_s = 666.66$, see Pelekasis (1991).

The response of the system when the motion is induced by an acoustic pressure field is presented in the following for several different values of the forcing frequency ω_f. The evolution of the shapes of the two bubbles with time follows a distinct pattern as ϵ increases for all the values of ω_f used. As a typical example the results for $\omega_f = 6.5$ and $D = 4$ are discussed next.

This value of the forcing frequency allows for either subharmonic resonance with P_2, or harmonic resonance with P_3. However, neither of these two effects is observed since

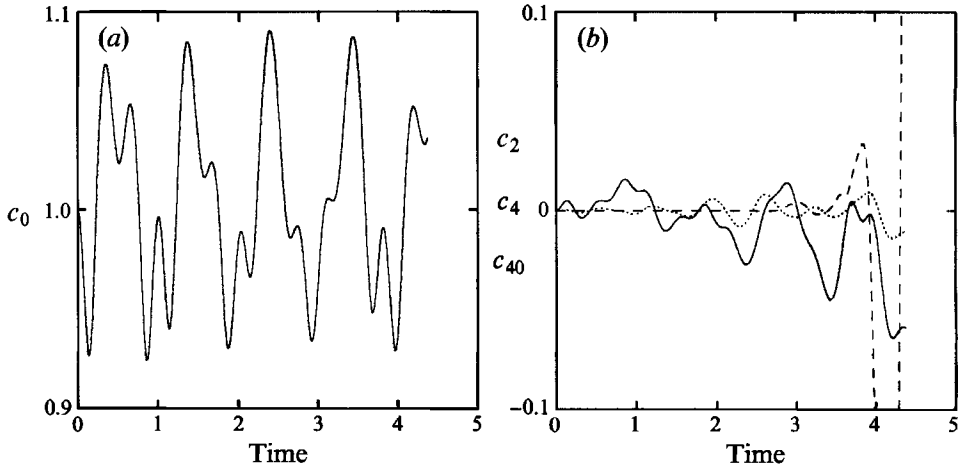

FIGURE 4. Variation with time of selected Legendre coefficients, (*a*) c_0, (*b*) ——, c_2; ..., c_4; – – –, c_{40}, of the shape of either bubble; $R = 1$, $D = 4$, $P_s = 50$, $\epsilon = 0.2$ and $\omega_f = 6.5$.

they are both preceded by other effects that evolve faster. When ϵ is 0.2 the two bubbles are seen to approach each other almost until coalescence. No significant deformations or instabilities appear even in the rear surfaces and computations proceed for a long time. The shape is dominated by P_0, and to a lesser extent by P_2, as shown in figure 4. As time increases and the two bubbles approach each other, the accuracy of computations decreases and short-wave growth does not allow the integration to proceed further. This growth of P_{40} and other high modes can be postponed, for example, by spatial and temporal refinement as discussed in Pelekasis *et al.* (1992). On the other hand, the superposition of the breathing mode and the oscillatory motion due to the acoustic disturbance is obvious in the variation of c_0, c_2 and c_3. Before computations fail c_4 and c_5 oscillate with periods of 0.68 and 0.62, respectively, while the nonlinear period of the breathing mode is found to be 0.35 approximately. Therefore, the inception of subharmonic resonance is detected. However, the current value of ϵ is too small for subharmonic resonance to become apparent in bubble shapes. The Bond number is also oscillating with too small an amplitude to produce any significant effect; its maximum value is 0.36. Therefore, neither spherical-cap shapes nor globally deformed shapes arise by the time computations fail ($t = 4.4$).

Increasing ϵ to 0.5 gives rise to spherical-cap shapes at $t \approx 1.1$, see Pelekasis (1991). *Bo* becomes 1.0 during the first period of volume oscillations and 1.6 during the second one. Thus, acceleration becomes the dominant effect, which eliminates any possibility for subharmonic resonance. The period of the oscillations of c_4 and c_5 has drifted away from twice the period of c_0, which is 0.25. A very interesting coupling of effects is observed when ϵ is set to 0.6. The familiar pattern of spherical-cap shapes arises at time $t \approx 0.9$, figure 5, in compliance with the $O(1/\epsilon)$ timescale. Nevertheless, before spherical-cap shapes appear the volume of the two bubbles increases and then drops rapidly, while the oscillations of P_0, shown in figure 6(*a*), exhibit a tendency for period doubling. Period doubling in spherosymmetric oscillations of a single bubble has been reported by Lauterborn (1976), and Lauterborn & Cramer (1981). Eventually the rest of the modes start growing as well, see Pelekasis (1991).

This subharmonic signal is even more evident in the oscillations of P_0 when $\epsilon = 0.8$. Counting the peaks in the variation of P_0 in figure 6(*b*) one finds that they occur at time $t = 0$, 0.306 and 0.668. Furthermore, a shallow minimum occurs at $t = 0.354$ and the

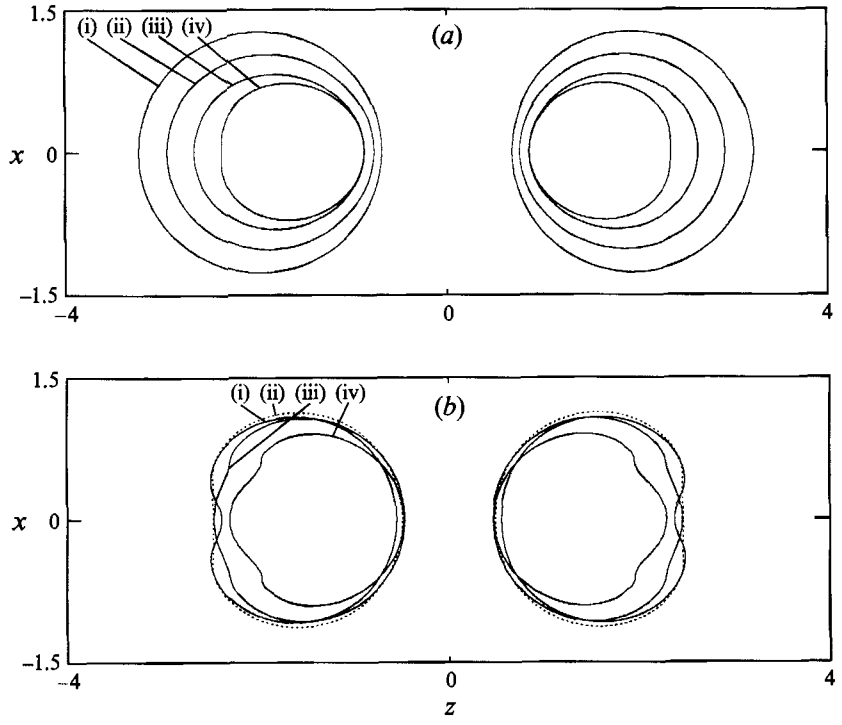

FIGURE 5. Bubble shapes, obtained up to breakdown of computations due to short-wave growth with $R = 1$, $D = 4$, $P_s = 50$, $\epsilon = 0.6$ and $\omega_f = 6.5$, at (*a*): (i) $t = 0.64$, (ii) $t = 0.76$, (iii) $t = 0.80$, (iv) $t = 0.84$; (*b*): (i) $t = 0.92$, (ii) $t = 0.96$, (iii) $t = 1.00$ and (iv) $t = 1.04$.

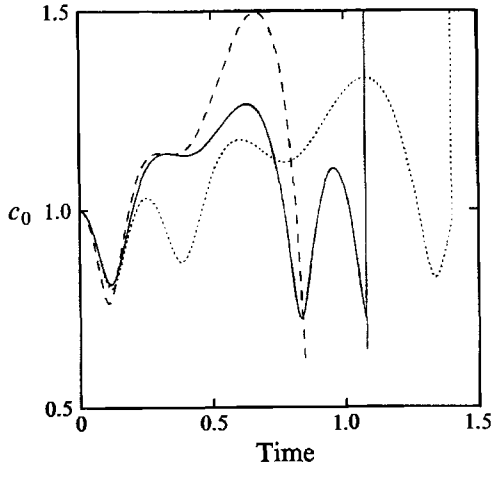

FIGURE 6. Variations with time of the zeroth Legendre mode, c_0, of the shape of either bubble; $R = 1$, $D = 4$, $P_s = 50$: (*a*) ——, $\epsilon = 0.6$, $\omega_f = 6.5$; (*b*) – – –, $\epsilon = 0.8$, $\omega_f = 6.5$; and (*c*) ..., $\epsilon = 0.6$, $\omega_f = 3.5$.

part of the curve between $t = 0.306$ and 0.354 almost forms a plateau. The rest of the modes do not grow significantly throughout the computation; see Pelekasis (1991). Comparing the variation of c_0 as obtained with $\epsilon = 0.6$ and 0.8, one notices that the portion around the second minimum is gradually eliminated and tends to be replaced

by a continuous line connecting the first minimum and maximum. This indicates that period doubling is about to take place. The shapes of the two bubbles exhibit a significant growth in volume followed by an explosive collapse.

The pattern for the response of the two bubbles described above is observed also for the following values of ω_f: 3.5, 5.0, 6.5 and 12. Namely, for $\epsilon \approx 0.2$, the two bubbles approach each other until coalescence without any significant deformation. Spherical-cap shapes appear for large enough values of ϵ, and subharmonic volume oscillations with bubble collapse dominate as ϵ increases even further. For example, when $\omega_f = 3.5$ and $\epsilon = 0.6$ the oscillations of P_0 shown figure 6(*c*) also exhibit minima at times $t = 0.119$, 0.384, 0.775 and 1.339. The last interval is 0.564 and is approximately twice the period of the breathing mode, 0.265, found from the first interval. Period doubling in this lower frequency takes a little longer to arise. Again the pattern of rapid volume change is observed. Nonetheless, eventually spherical-cap shapes dominate. The evolution of the rest of the modes is given in Pelekasis (1991). When ϵ is set to 0.8 collapse of volume occurs before any significant deformation appears on the two interfaces. In order to examine the large-amplitude response of the two bubbles when they are driven above resonance, the frequency of the acoustic pressure field was set to $\omega_f = 30 > \omega_0 = 18.5$ and its amplitude to 0.8. The severe volume oscillations observed above are eliminated and the familiar pattern of spherical-cap shapes dominates. It seems that now that the timescale associated with the forcing, $T_f = 2\pi/\omega_f$, is smaller than the period of the breathing mode, the motion is determined by the former and the subharmonic signal in the volume oscillations is not present.

It is noteworthy that when the subharmonic signal is observed in the oscillations of P_0, it is with respect to the breathing mode and not the forcing frequency. This is in agreement with the early calculations of Flynn (1964) for the radial motion of a single bubble under the influence of an acoustic pressure field. The same result was used later by Neppiras (1969) in explaining the subharmonic signal emitted by liquids in acoustic cavitation experiments.

When the two bubbles are further apart, $D = 10$, and the other parameters are kept the same as in the previous section, the possibility for spherical-cap shapes is eliminated, since $\langle g \rangle$ decreases with D^2 (Part 1) and it is calculated here to remain below the required threshold. Consequently, the remaining competing effects are due to resonance between the breathing mode or the forcing and the Legendre modes.

Introducing an oscillatory pressure disturbance at infinity, with frequency $\omega_f = 3.5$ and amplitude $\epsilon = 0.6$, gives rise to five-lobed shapes as a result of subharmonic resonance between the breathing mode and P_4, P_5 and P_6. Monitoring of the evolution of the Legendre coefficients of the latter modes, just before computations fail, gives their oscillation period to be roughly double that of the breathing mode. Further increase of ϵ to 0.8 causes subharmonic excitation of P_0 accompanied by rapid volume growth and collapse, figure 7. No modes higher than the third seem to be excited during this motion.

Finally, it should be noted that decreasing ϵ to 0.3 decelerates the growth of P_4 and P_5 that was seen to occur through resonance with the breathing mode. At the same time increasing ω_f to 7.0 allows subharmonic resonance between the acoustic field and P_2. Computations proceed for a long time without large deformations in shape. However, important information can be inferred from the variation of the Legendre coefficients. As can be seen from figure 8, c_0 is participating in two periodic motions. The fast one is identified as the breathing mode with period 0.32, whereas the slow one is due to the acoustic pressure field with period 0.9. The fast motion is evident in the oscillations of P_2 as well. P_2 is also engaged in a second periodic motion which completes three periods

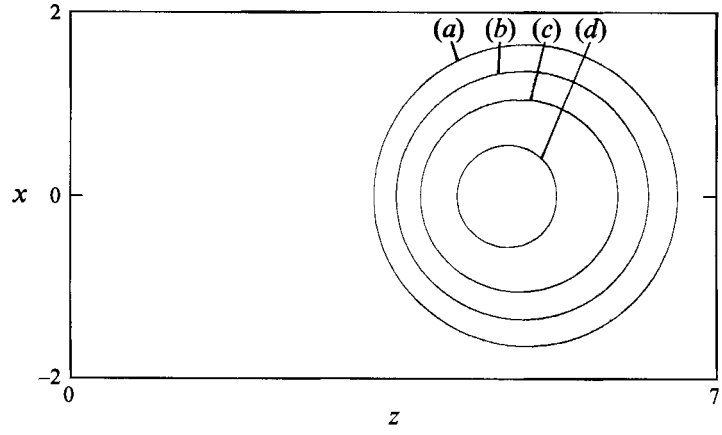

FIGURE 7. Bubble shapes, obtained up to breakdown of computations when $R = 1$, $D = 10$, $P_s = 50$, $\epsilon = 0.8$ and $\omega_f = 3.5$, at (*a*) $t = 1.20$, (*b*) $t = 1.28$, (*c*) $t = 1.32$ and (*d*) $t = 1.36$.

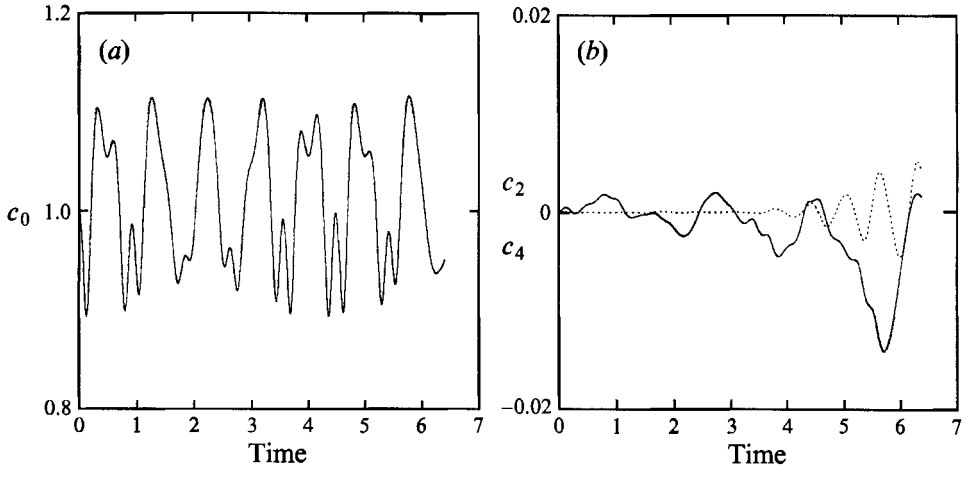

FIGURE 8. Variation with time of selected Legendre coefficients, (*a*) c_0, (*b*) ——, c_2; ..., c_4, of the shape of either bubble; $R = 1$, $D = 10$, $P_s = 50$, $\epsilon = 0.3$ and $\omega_f = 7.0$.

in the time interval shown in figure 8(*b*). Counting the distance between the maxima defining these three time intervals results in a period of approximately 1.8, indicating subharmonic resonance with the acoustic sound field for the first time. The amplitude of this periodic motion increases almost exponentially with time. At the same time P_4, P_5 and P_6 are growing through subharmonic resonance with the breathing mode with a period of approximately 0.64. Unfortunately, simultaneous growth of high modes deteriorates the accuracy of computations; see Pelekasis (1991). Thus, it is not possible to follow the motion further and verify whether one of the two subharmonic resonances will eventually dominate before coalescence.

5. Motion of bubbles of unequal size due to a step change in pressure

Before examining the more complicated response of unequal bubbles to an oscillatory pressure field it is instructive to examine their response to a step change in pressure with $P_s = 666.66$. Since $R < 1$ it is anticipated that their motion and

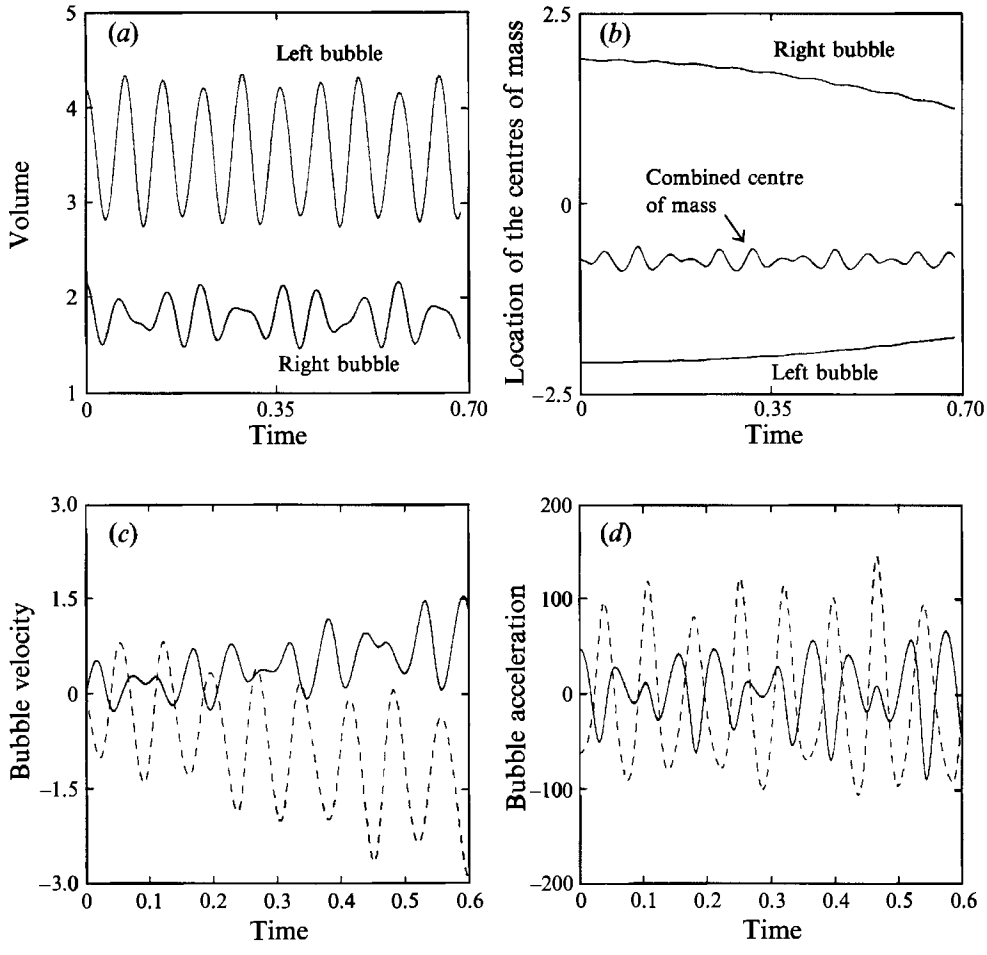

FIGURE 9. (*a*) Volume oscillations of each bubble; (*b*) evolution of the centres of mass of mass of each bubble and the combined centre of mass of the two bubbles; (*c*) variation with time of the velocity of the left (——) and right (– – –) bubble, and (*d*) variation with time of the acceleration of the left (——) and right (– – –) bubble. Parameter values are $R = 0.8$, $D = 4$, $\epsilon = 0.3$ and $P_s = 666.66$.

deformation will involve the two distinct sets of eigenmodes predicted by linear theory, see Part 1. More specifically, in the first set of modes the two bubbles oscillate with a frequency close to one of the eigenfrequencies of the left bubble alone; the left bubble deforms, while the right one remains almost spherical. In the other set of modes it is the right bubble that deforms most and the frequency is similar to one of its eigenfrequencies in the absence of the bubble on the left. Hence, two sets of timescales will be involved in their combined motion, with the two eigenmodes corresponding to volume oscillations of the left or right bubble being dominant (zeroth modes).

This is shown in figure 9 for two bubbles of radii ratio of $R = 0.8$, with $D = 4$, and for amplitude of the initial disturbance $\epsilon = 0.3$. The volumes of the two bubbles undergo large-amplitude oscillations, figure 9(*a*). This primary motion induces attraction between the two bubbles, as can be seen by the motion of the two centres of mass, figure 9(*b*). The combined centre of mass, Z, as defined in Part 1, is not constant any more, but it fluctuates around its value at $t = 0$. The velocity and acceleration of the centres of mass of each bubble are shown in figure 9(*c*, *d*) to

oscillate in time. It is important to note that the extrema in the velocity and acceleration of the translatory motion of one bubble occur at points in time dictated by the volume oscillations of the other one. This clearly demonstrates that acceleration in one bubble is induced by volume oscillations of the other one, see Part 1.

By counting the maxima in the volume oscillations it is observed that there is no easily identifiable unique period. However, the time it takes for three consecutive maxima to appear in the volume oscillations of the left bubble and for five consecutive maxima to appear in the volume oscillations of the right bubble, seems to be constant and is found to be roughly 0.15 and 0.21, respectively. Taking the average acceleration over the time interval 0.21 for the left bubble and the time interval 0.15 for the right bubble, gives the familiar pattern of approximately constant, attractive acceleration, initially, with a tendency to decrease towards the later stages. The actual values for the average acceleration are about 1.47 and 2.8 initially, corresponding to the left and right bubble. The ratio of accelerations is roughly the inverse of the ratio of bubble volumes, which in this case is $V_1/V_2 = 1.953$. Therefore, the smaller bubble is moving faster since it behaves as a body of less inertia compared to the larger one. Both values of acceleration given above are smaller than the value 4.1 obtained under the same conditions but when $R = 1$, see figure 9 in Part 1. This is attributed to the fact that the interaction force between the two bubbles is smaller now that they are displacing a smaller amount of fluid.

This result is better understood in the context of the Kelvin impulse. More specifically, it was shown by Blake & Cerone (1982) that in the absence of any boundary at a finite distance from a number of material surfaces the sum of Kelvin impulses on all the surfaces is time independent. In the present study the total Kelvin impulse is zero initially and in view of the above theorem does not change with time. As a result, the two bubbles will experience a force equal in size, but acting in opposite directions. Consequently, the one occupying the smaller volume will acquire a larger acceleration. The virtual mass would be a more appropriate quantity to use instead of the volume; however, this would only change the average acceleration by a constant. Therefore the volume ratio will be approximately inversely proportional to the ratio of the two average accelerations.

For bubbles of unequal size, the Bond number remains equal to the average dimensionless acceleration $\langle g_1 \rangle$ for the bubble on the left; whereas it is $Bo = \langle g_2 \rangle R^2$ for the bubble on the right. For the case discussed above the individual Bond numbers are 1.47 and 1.792 for the left and right bubble, respectively. Consequently, the left bubble is expected to undergo shape oscillations which will eventually manifest themselves everywhere on the interface, whereas the right bubble is expected to give rise to spherical-cap shapes. Indeed, this can be seen in figure 10, where shapes are shown until computations break down for the reasons given in Part 1. The dominant modes of the bubble on the left at time 0.68 are P_9 and P_{10}, whereas the free surface on the right bubble deforms only at its rear side with P_2 being the dominant mode.

Increasing the radii ratio, R, increases the average acceleration of the two bubbles and the individual values of Bo, until at some point both bubbles exhibit spherical-cap shapes, similarly to the case with equal radii. For example, when $R = 0.95$ both bubbles behave in this way and the right one does so faster owing to its slightly larger Bond number.

On the other hand decreasing R decreases Bo as well, but the bubbles are still moving towards each other. For the parameter values $R = 0.7$, $D = 4$, and $\epsilon = 0.3$ even the right bubble ceases to exhibit spherical-cap shapes, figure 11, and, until the computation fails at $t = 0.64$, it does not deform significantly. The left bubble evolves

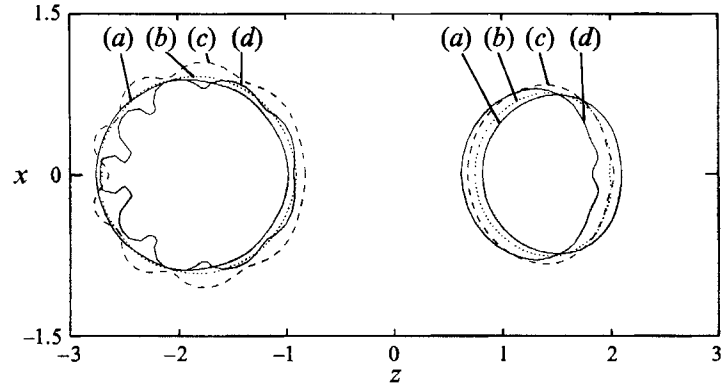

FIGURE 10. Bubble shapes, obtained up to breakdown of computations with $R = 0.8$, $D = 4$, $\epsilon = 0.3$ and $P_s = 666.66$, $\omega_f = 0$, at (*a*) $t = 0.54$, (*b*) $t = 0.60$, (*c*) $t = 0.64$ and (*d*) $t = 0.68$.

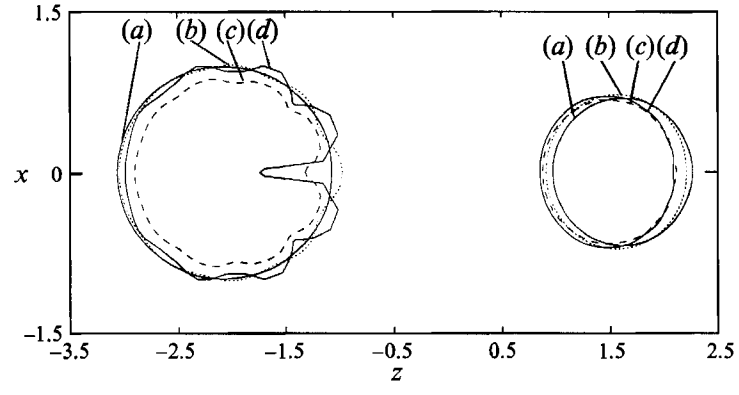

FIGURE 11. Bubble shapes obtained up to breakdown of computations with $R = 0.7$, $D = 4$, $\epsilon = 0.3$ and $P_s = 666.66$, $\omega_f = 0$, at (*a*) $t = 0.50$, (*b*) $t = 0.56$, (*c*) $t = 0.60$ and (*d*) $t = 0.64$.

as before but its acceleration is much smaller. Monitoring the acceleration of the two bubbles as described in the previous case, we find that the average acceleration of the left bubble is roughly 0.7, whereas the average acceleration of the right bubble is 1.8 ($Bo = 0.882$). Again the ratio of the two accelerations, $\langle g_1 \rangle / \langle g_2 \rangle = 0.388$, is roughly the inverse of the ratio of the two volumes, $V_1/V_2 = 2.915$. In other words, the forces exerted by the fluid on the two bubbles as a result of their oscillations are approximately the same.

As mentioned at the end of § 5 in Part 1 acceleration stabilizes the side facing in its direction. However, when the entire interface deforms, with Bo below the critical range, even this side starts deforming albeit later in time and less than the other side, see figure 10. On the other hand, when acceleration of both bubbles is further decreased, its stabilizing effect is not as pronounced; see shapes obtained for $R = 0.7$ in figure 11. Towards the late stages of motion the left bubble exhibits globally deformed shapes with nine well-defined lumps appearing even on its front side, while the right bubble is undergoing volume oscillations as predicted by linear theory. The mechanism that gives rise to such shapes is again subharmonic resonance between the breathing mode of the left bubble and P_9 and P_{10}. This is explained in Pelekasis (1991) by decomposing

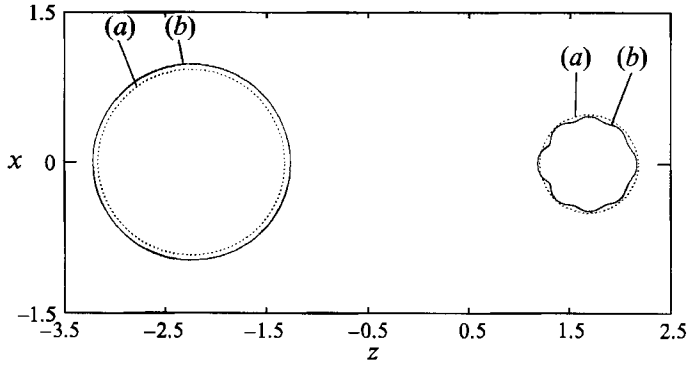

FIGURE 12. Bubble shapes, obtained up to breakdown of computations with $R = 0.5$, $D = 4$, $\epsilon = 0.3$ and $P_g = 666.66$, $\omega_f = 0$, at (*a*) $t = 0.30$ and (*b*) $t = 0.36$.

the shape of the two bubbles in Legendre polynomials and considering their eigenfrequencies.

It was shown in Part 1 that the time needed for such globally deformed shapes to become evident on the left bubble is $O(1/\epsilon)$. Indeed, when computations for $R = 0.7$ are repeated with a smaller value of $\epsilon = 0.2$ the same behaviour is observed later in time, $t = 0.9$, as opposed to $t = 0.6$ when $\epsilon = 0.3$. There is also the possibility of harmonic resonance between the breathing mode and one of the even higher Legendre modes. However, the time needed for such an effect to become apparent is $O(1/\epsilon^2)$. Thus, subharmonic resonance occurs faster and does not allow for harmonic resonance to evolve. This pattern has been observed on several different occasions in Part 1 as well as the present study.

Moreover, now that the acceleration of the left bubble is much smaller compared to the case with $R = 0.8$, a liquid jet is seen to penetrate its surface from the front. This occurs shortly before computations collapse and after the appearance of globally deformed shapes. Jet formation in accelerating bubbles in the vicinity of other surfaces has also been reported by Blake & Gibson (1981). They found that during interaction between a vapour cavity and a gas/liquid interface, a jet is formed on the bubble side closer to the interface, whereas it is formed on the bubble side further away from a solid/liquid interface. In both cases the ensuing jet leads to bubble collapse. However, only the former case is relevant here and it is indeed observed. It should be noted, that the size and velocity of the jets observed throughout this study are smaller and appear later than in Blake & Gibson (1981) and in Blake, Taib & Doherty (1986). This is because in their case the Kelvin impulse is always towards the cavity, whereas here it oscillates following the volume oscillations of each compressible bubble.

Further decrease of the radii ratio R to 0.5, and keeping $\epsilon = 0.3$ and $D = 4$, decreases the average acceleration of the two bubbles to 0.16 and 1.0 for the left and right bubble, respectively. $Bo = 0.25$ for the right bubble and the ratio $\langle g_1 \rangle / \langle g_2 \rangle = 0.16$ is quite close to the ratio $V_2/V_1 = 0.125$ of the two volumes. Therefore, to an outside observer the smaller bubble will appear to accelerate almost ten times faster than the larger one. As can be seen from figure 12 it is the smaller bubble that exhibits rapid shape oscillations and global deformation, in contrast to the case with $R = 0.7$ when it was the left bubble. This is because now the acceleration of both bubbles is below the threshold and both may exhibit globally deformed shapes. However, the higher frequency of the zeroth mode of the smaller right bubble leads to faster interaction with its harmonics. In particular, the required relation for subharmonic resonance holds for

the P_8 and P_9 modes of the right bubble ($\omega_{0,r} \approx 153.2$, $\omega_8 \approx 70.9$, and $\omega_9 \approx 83.9$ when $R_2 = 0.5$; whereas $\omega_{0,l} \approx 74.5$, $\omega_{10} \approx 34.5$ and $\omega_{11} \approx 39.5$ when $R_1 = 1$).

For all cases examined the Bond number of the smaller bubble is always found to be greater than that of the larger bubble. This indicates that the average acceleration of the left bubble, $\langle g_1 \rangle$, decreases faster than R^2 when $R \to 0$. In fact, the accelerations calculated during the beginning of the motion for $D = 4$, $\epsilon = 0.3$ and $P_s = 666.66$ when $R = 0.8, 0.7, 0.5$, are: $(\langle g_1 \rangle, \langle g_2 \rangle) = (1.47, 2.8)$, $(0.7, 1.8)$ and $(0.16, 1.0)$, respectively. These values show that $\langle g_2 \rangle$ decreases roughly like R^2; whereas, $\langle g_1 \rangle$ decreases faster than R^4.

6. Bubbles of unequal size in an oscillatory pressure field.

6.1. *General characteristics*

In their study on acoustic cavitation Kornfeld & Suvorov (1944) argued, that it follows from the general theory of vibrations that the pulsations of a pair of bubbles must either coincide in phase or be in opposite phases. According to them, this should depend upon whether the size of these bubbles is on the same or different sides of the resonant size corresponding to the forcing frequency. Consequently in the context of Bjerknes forces one obtains that, if the forcing frequency lies in the interval between the two eigenfrequencies for volume oscillations, the two bubbles repel each other, whereas the forces between the two bubbles are attractive in any other case. In the following we will verify this behaviour and see how it is coupled with the effects described earlier. To this end, we compute the response of two bubbles to an oscillatory acoustic pressure for a wide range of forcing frequencies.

Introducing an oscillatory pressure change at infinity adds one more timescale in the volume oscillations of both bubbles and increases the possibilities for resonance. Nevertheless, as can be seen from table 1 in Part 1 and (3.1) and (3.2) here, when $P_s = 666.66$ the frequency of the first ten Legendre modes is much smaller than the natural frequency for volume oscillations. Consequently, when $\omega_f < \omega_{0,l}, \omega_{0,r}$ the time needed for one of these modes to grow through subharmonic resonance with the acoustic pressure is much larger than the time needed for the breathing modes to excite them. On the other hand, when the forcing frequency significantly exceeds the natural frequency of either bubble ($\omega_f > \omega_{0,l}, \omega_{0,r}$) subharmonic resonance between the forcing and one of the higher Legendre modes, $P_k, k \geqslant 15$, is possible and is indeed found.

6.2. *Effect of varying the forcing frequency*

Two different values of the radii ratio were used; $R = 0.5, 0.7$. Results obtained with $R = 0.7$ only are presented here; those obtained with $R = 0.5$ along with more details are given in Pelekasis (1991). The dimensionless static pressure is set to 666.66, the dimensionless initial distance between the two centres of mass $D = 4$, and the amplitude of the acoustic pressure $\epsilon = 0.3$ for all cases, unless otherwise indicated.

First, values of ω_f are examined that are smaller than either of the breathing mode frequencies. Taking $\omega_f = 3.5$, the volume of the left bubble is oscillating with a period of 0.08 and slowly increasing amplitude. The volume of the right bubble is also slowly increasing while it is oscillating with a period of 0.05 and amplitude slowly increasing in time, Pelekasis (1991). The values of the individual periods deviate slightly from those calculated using linear theory, but follow the $R^{\frac{3}{2}}$ dependence stated in §3. The total energy is oscillating with the same frequency as the far-field pressure. Owing to the appearance of the shape instability on the left bubble computations proceed for only half a period of the acoustic pressure. Figure 13 shows the motion of the centres

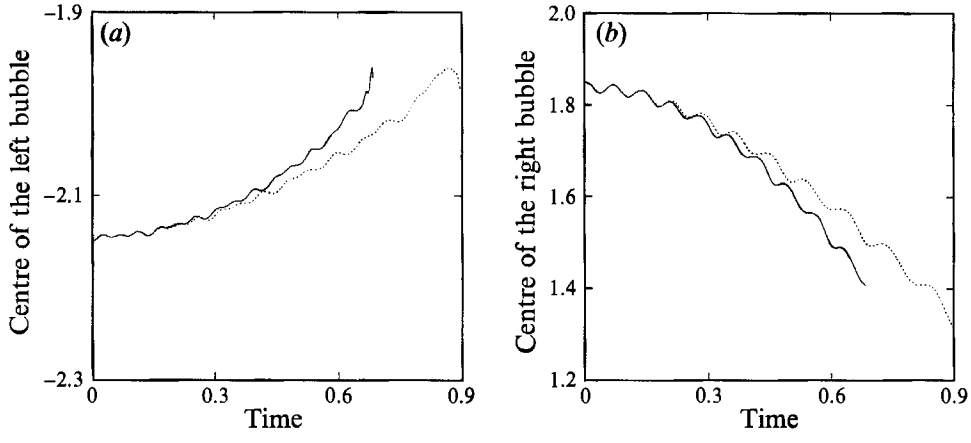

FIGURE 13. Evolution of the centre of mass of (*a*) the left and (*b*) the right bubble for a step change in pressure, $\omega_f = 0$ (——), and for an oscillatory pressure change at infinity, $\omega_f = 3.5$ (...); $R = 0.7$, $D = 4$, $P_g = 666.66$ and $\epsilon = 0.3$.

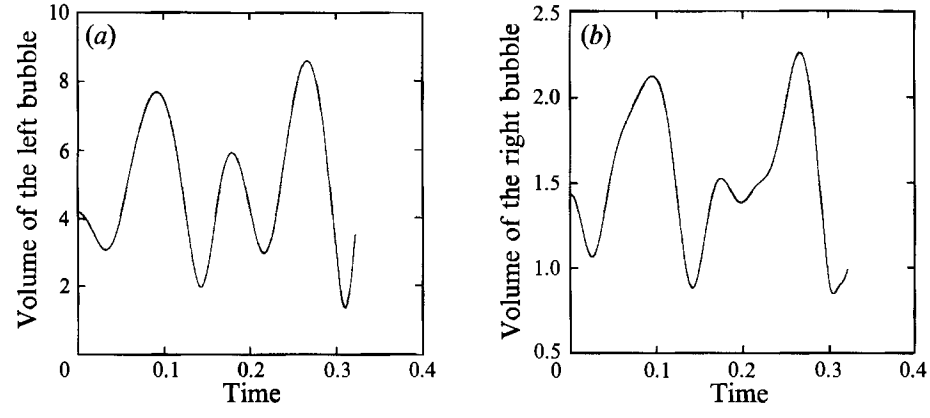

FIGURE 14. Variation with time of the volume of (*a*) the left and (*b*) the right bubble; $R = 0.7$, $D = 4$, $P_g = 666.66$, $\epsilon = 0.3$ and $\omega_f = 40$.

of mass of the two bubbles for both a step change in pressure ($\omega_f = 0$) and for $\omega_f = 3.5$. In the latter case the acceleration of the two bubbles is smaller, hence the time needed for shape oscillations to arise is larger, see Pelekasis (1991). This is attributed to the fact that when the energy is varying in the far field the available energy in the system oscillates as well. Consequently any long-time effect that is about to evolve in one direction during the first half of the period of the external forcing is reversed in the second half, thus generating a weaker net effect than in the case of a step change. It is also interesting to note that the forcing frequency is very close to the linear frequency of P_2. However, harmonic resonance does not have enough time to evolve.

Increasing ω_f to 40, which is roughly half the natural frequency of the left bubble, changes the picture significantly. The total energy of the system follows (2.4) very closely and is still oscillating with the frequency of the forcing but this time with increasing amplitude, see Pelekasis (1991). Similarly the amplitude of the volume oscillations of the left bubble increases significantly owing to superharmonic resonance between the forcing and the breathing mode, figure 14. These large vibrations of the left bubble force the right bubble to accelerate faster and spherical-cap shapes appear

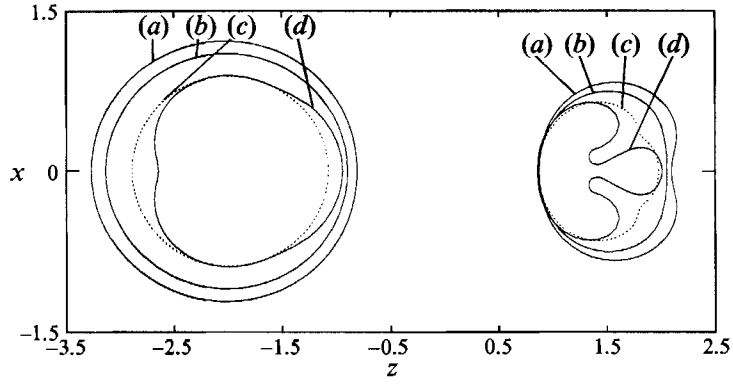

FIGURE 15. Bubbles shapes obtained up to breakdown of computations with $R = 0.7$, $D = 4$, $P_a = 666.66$, $\epsilon = 0.3$ and $\omega_f = 40$, at (*a*) $t = 0.28$, (*b*) $t = 0.29$, (*c*) $t = 0.30$ and (*d*) $t = 0.32$.

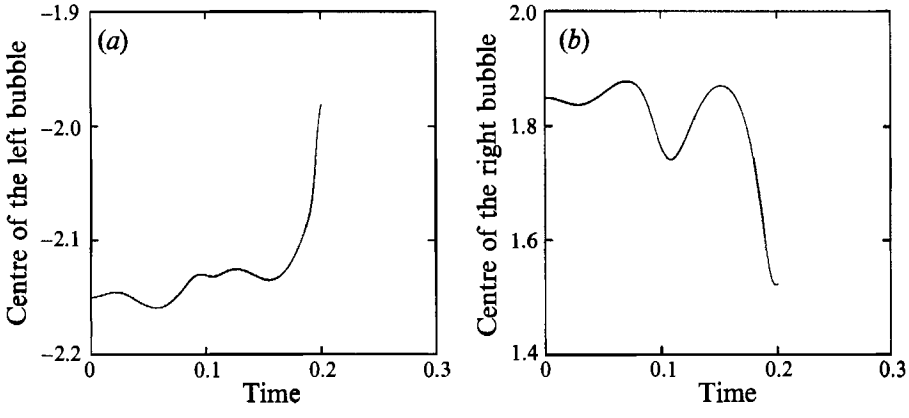

FIGURE 16. Variation with time of the centres of mass of (*a*) the left and (*b*) the right bubble under conditions of resonance between the forcing frequency and the breathing mode of the left bubble; $R = 0.7$, $D = 4$, $P_a = 666.66$, $\epsilon = 0.3$ and $\omega_f = 73.5$.

before even the left bubble exhibits any significant deformation, figure 15. Decreasing ϵ to 0.2 postpones the appearance of such shapes until $t = 0.519 (\approx 0.32\frac{0.3}{0.2})$, which conforms with the $O(1/\epsilon)$ scaling for the effect of acceleration found in Part 1.

The evolution of the centres of mass of the two bubbles when ω_f is set to be the same as the linear frequency of the breathing mode of the left bubble, 73.5, is different. Under these near-resonance conditions, it is not clear whether attractive or repulsive forces will prevail. Indeed, initially the two centres of mass are seen in figure 16 to oscillate intensively around their position at $t = 0$ without exhibiting any net displacement. However, they eventually accelerate very fast towards each other owing to the presence of a very small yet important detuning between the forcing frequency and the zeroth frequency of the left bubble. The volume of the left bubble expands and then shrinks very rapidly, whereas its shape remains pretty much spherical. As an indication of the criticality of the situation and the intense oscillation of the centre of mass of the right bubble, it initially tends to form spherical-cap shapes on the side away from the (x, y)-plane, but when the motion is reversed it starts deforming on the other side as well, see figure 17.

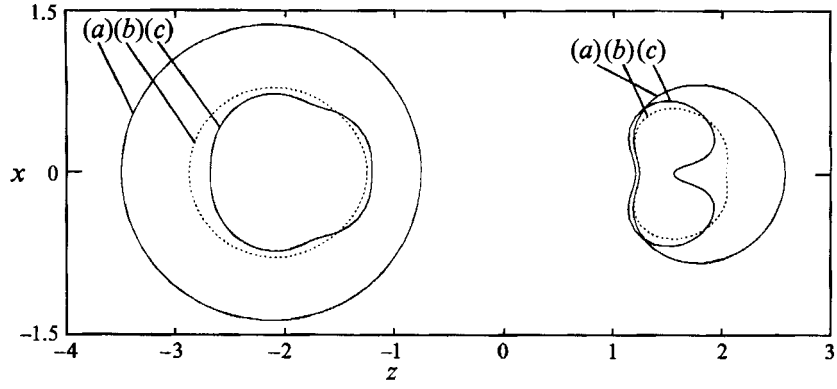

FIGURE 17. Bubble shapes, obtained up to breakdown of computations with $R = 0.7$, $D = 4$, $P_s = 666.66$, $\epsilon = 0.3$ and $\omega_f = 73.5$, at (*a*) $t = 0.16$, (*b*) $t = 0.19$, and (*c*) $t = 0.20$.

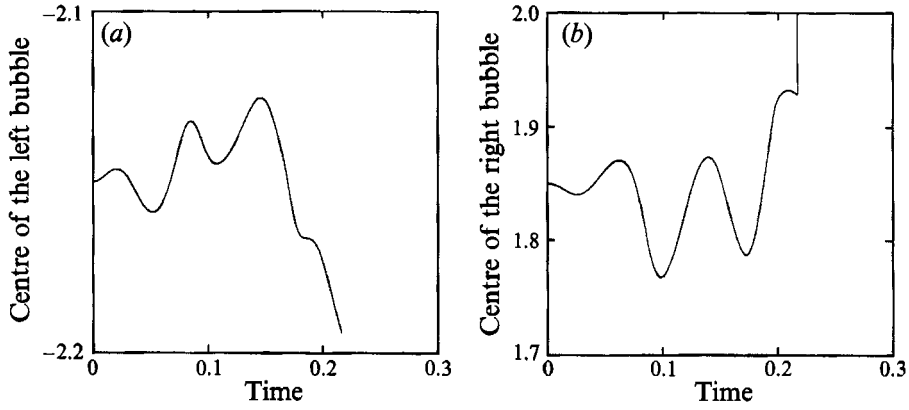

FIGURE 18. Variation with time of centre of mass of (*a*) the left and (*b*) the right bubble; $R = 0.7$, $D = 4$, $P_s = 666.66$, $\epsilon = 0.3$ and $\omega_f = 90$.

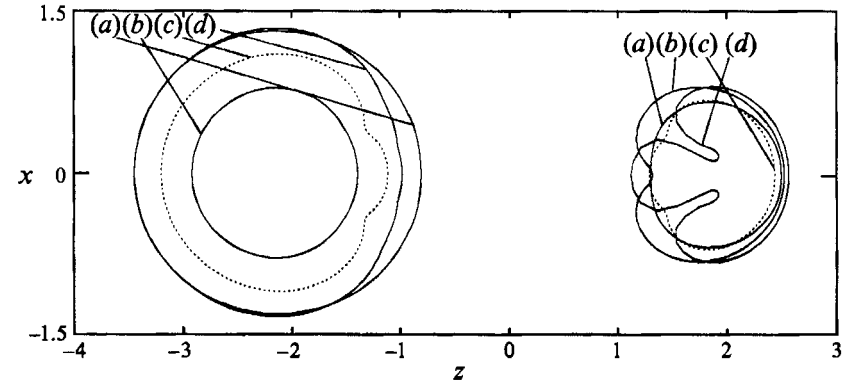

FIGURE 19. Bubble shapes obtained up to breakdown of computations with $R = 0.7$, $D = 4$, $P_s = 666.66$, $\epsilon = 0.3$ and $\omega_f = 90$, at (*a*) $t = 0.14$, (*b*) $t = 0.17$, (*c*) $t = 0.19$ and (*d*) $t = 0.21$.

With ω_f between the breathing frequencies of each bubble, a repulsive force should develop. Indeed, increasing ω_f to 90 makes the two bubbles repel each other, as can be seen from figure 18. The amplitude of the volume oscillations of the left bubble is still large and the right bubble exhibits spherical-cap shapes. Of course, now that the

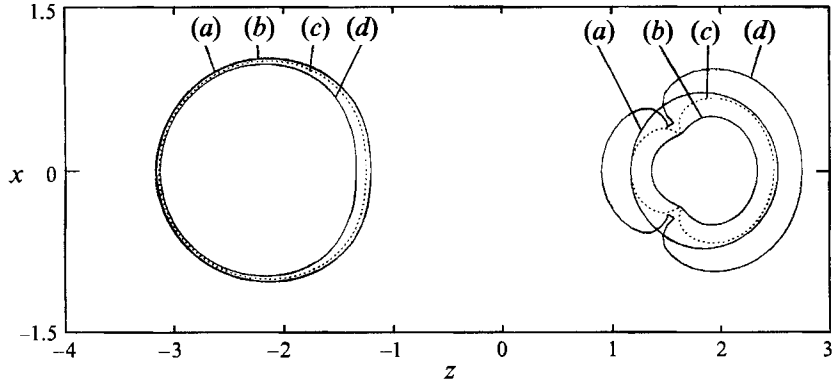

FIGURE 20. Bubble shapes obtained up to breakdown of computations with $R = 0.7$, $D = 4$, $P_a = 666.66$, $\epsilon = 0.3$ and $\omega_f = 111.7$, at (*a*) $t = 0.175$, (*b*) $t = 0.185$, (*c*) $t = 0.190$ and (*d*) $t = 0.200$.

acceleration is in the opposite direction from before, deformations appear on the side closer to the (x, y)-plane, figure 19.

Increasing ω_f further may cause resonance between the forcing and breathing mode of the right bubble. This should happen when $\omega_f = 111.7$. After an initial stage of intense oscillatory motion the centres of mass of the two bubbles eventually move away from each other, see Pelekasis (1991). Computations fail owing to the severe volume oscillations of the right bubble. The left bubble does not deform significantly, while the right one is dominated by the P_2 and P_3 modes, figure 20. Comparing the two cases in which direct resonance of the left or right bubble should be expected (figure 17 *vs.* figure 20) we find that in both cases the smaller bubble accelerates and deforms the most, whereas the bubble in direct resonance with ω_f exhibits the largest volume oscillations. The slight detuning caused by nonlinearities in the first case results in attractive forces and in the second case in repulsive forces.

Moving away from the interval between the natural frequencies of the two breathing modes, allows the attractive forces between the two bubbles to prevail again. By setting $\omega_f = 180$ both bubbles stop exhibiting violent volume oscillations and the right bubble assumes globally deformed shapes. In fact it turns out that the linear frequencies of P_{13} and P_{14} for $R_2 = 0.7$, as given by (3.1), are 85 and 95 respectively. This indicates the possibility of subharmonic resonance between the forcing and the above modes. Indeed, the right bubble is gradually developing 13 lumps, as can be seen from figure 21. This signals the onset of shape oscillations and decomposition of the shape of the right bubble in spherical harmonics gives P_{15} as the dominant higher mode. Counting the distance between the peaks in the oscillations of c_{15} we find that towards the end of the computations the period of its variation is roughly 0.0665 which is approximately twice the period of the forcing, $2\pi/\omega_f = 0.035$. Subharmonic resonance between the breathing mode of the left bubble and P_9, P_{10} and P_{11} is also possible, but it does not have time to evolve since the period of these modes is larger than the period of the modes resonating with the acoustic field. Variation with time of the most important Legendre modes is given in Pelekasis (1991). Repeating the computation with $\epsilon = 0.2$ gives rise to the same effect at time $t = 0.95$, which is in accord with the $O(1/\epsilon)$ behaviour predicted by Hall & Seminara and verified numerically in Part 1.

A number of very interesting experimental observations have been reported by Crum & Nordling (1972). They produced transient cavities by applying an acoustic stationary wave of very large amplitude ($\epsilon = 4$) and frequency 55 kHz. They observed very rapidly

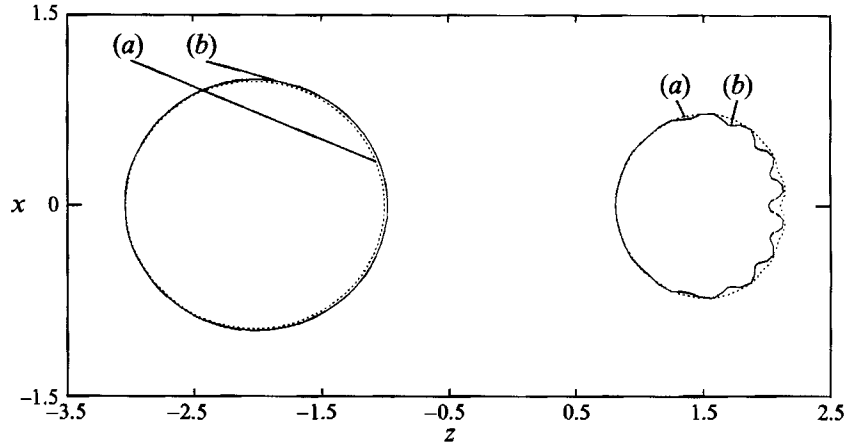

FIGURE 21. Bubble shapes obtained up to breakdown of computations with $R = 0.7$, $D = 4$, $P_a = 666.66$, $\epsilon = 0.3$ and $\omega_f = 180$, *at* (*a*) $t = 0.59$ and (*b*) $t = 0.62$.

deforming bubbles of velocity up to 1 m/s and lifetimes up to 10 ms under a strobelight. The accelerating bubbles were annihilated upon reaching their maximum velocity and formed smaller ones that would either break up again or move as a group. We believe that our calculations predict the same behaviour. Namely, after some time the accelerating bubbles develop a hydrodynamic instability that breaks them up exponentially fast. Although bubbles in these experiments achieve greater accelerations than in our calculations (the primary Bjerknes force is greater than the secondary one, Crum 1974) a qualitative agreement with the above data is readily obtained. The forced oscillations in figure 21 correspond to $\omega_f^* = 51$ kHz. Hydrodynamic instability arises in the right bubble at $t^* = 2.5$ ms. The average motion of the bubbles with the parameters given in figure 21 should not be too different from that reported in figure 9. In this fashion we find that just before instability occurs, the left and right bubble achieve velocities of 0.29 m/s and 0.51 m/s respectively.

7. Concluding remarks

The motion of two bubbles when a disturbance in the far-field pressure is applied in the form of an acoustic pressure field is examined here. The change in pressure induces volume oscillations of the two bubbles characterized by three timescales: the two individual periods of the linear volume oscillations of each bubble, the so-called breathing modes, and that of the forcing. At the same time the presence of the other bubble causes each bubble to accelerate in a slow timescale along their common axis of symmetry. This acceleration is known as the 'Bjerknes effect' and, irrespective of the original disturbance, it induces a force on the left bubble for example, F_1, which is very similar to that given by Newton's law of universal attraction,

$$F_1 \sim V_1\langle g_1\rangle \sim V_1(V_2/D^2). \tag{7.1}$$

In other words, F_1 is proportional to the mass (volume) of fluid displaced by the left bubble, V_1, times the induced average acceleration, $\langle g_1\rangle$. The latter is proportional to the volume of the fluid displaced by the right bubble, V_2, and inversely proportional to D^2. Moreover, $\langle g_i\rangle$, is proportional to ϵ^2, and depends on the relative size of the bubbles, R, and the phase difference in their volume oscillations.

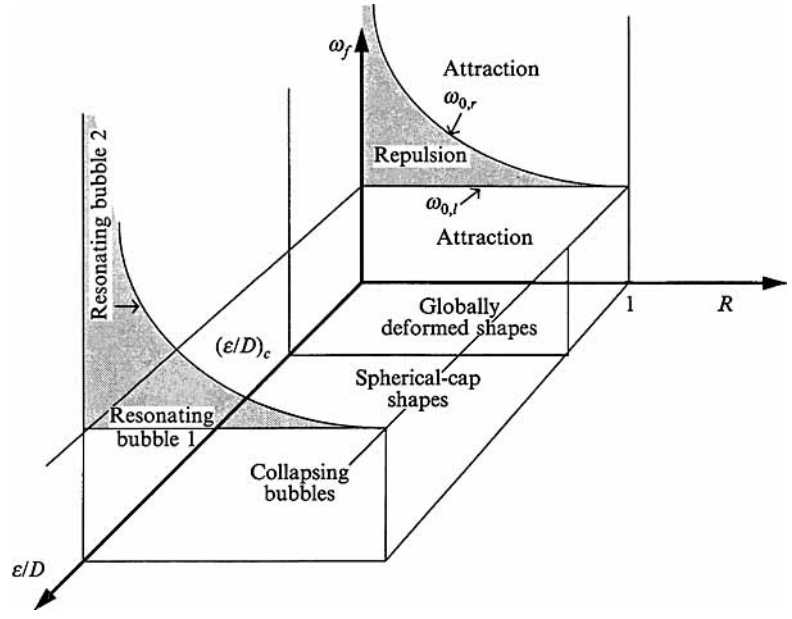

FIGURE 22. Schematic of the dynamic behaviour of two oscillating bubbles for different ranges of the operating parameters, ϵ/D, R and ω_f.

The wealth of observed phenomena can be better summarized by referring to figure 22. For any ambient pressure, the linear results by Bjerknes are confined on the plane with $\epsilon/D = 0$. When the dimensionless radii of the left and right bubbles are set at 1 and $R(\leqslant 1)$ respectively, their corresponding breathing-mode frequencies will remain constant and increase when $R \to 0$, see (3.2). Then, according to the linear result, bubble repulsion is possible only when $\omega_{0,l} < \omega_f < \omega_{0,r}$. The linear result is valid only for short times and increasing the amplitude of the disturbance pressure or decreasing the distance between bubbles increases bubble interaction. Thus, the ratio ϵ/D is used in figure 22 as a measure of nonlinearity. In general, bubble acceleration and harmonic resonance are the two competing nonlinear effects. Given the rest of the parameters, intermediate but large enough values of the amplitude ϵ induce resonance between either of the breathing modes, or the acoustic sound field and certain non-spherical Legendre modes. This can be harmonic or subharmonic. However, the former effect is not normally observed since it occurs on an $O(1/\epsilon^2)$ timescale. Subharmonic resonance occurs on an $O(1/\epsilon)$ timescale and is commonly captured in experiments and calculations. It gives rise to bubble shapes that are deformed everywhere on their surface and are dominated by the resonating modes. We have called such shapes globally deformed. Between the two periodic motions associated with volume oscillations the one with the higher frequency is more likely to cause subharmonic resonance, since the time needed for this effect to develop is less when the period of the basic motion is smaller.

Increasing ϵ further increases the relative importance of acceleration of the centre of mass, as compared with subharmonic resonance, until at some point a critical range of the average acceleration is exceeded. This is schematically indicated by the surface located at $(\epsilon/D)_c$ in figure 22. The corresponding critical Bond numbers have been reported for various conditions. Then, the stronger convection modifies the shapes obtained, which now resemble spherical-cap shapes. They occur on an $O(1/\epsilon)$ timescale as well.

Further increase of ϵ to significantly larger values, on the order of 0.8, generates a subharmonic signal in the oscillations of P_0 at half the frequency of the breathing mode. The shape of both bubbles is dominated by P_0, whereas significant volume growth is observed followed by rapid collapse. This behaviour is called transient cavitation and is often observed in cavitation experiments (Neppiras 1969). It should be noted that in the present study this effect is only observed when the forcing frequency is non-zero but below the frequency of the breathing mode of both bubbles.

For bubbles of unequal size, in addition to the previously mentioned effects, the direction of acceleration changes depending on the frequency of the pressure variation at infinity. More specifically, if ω_f lies in the interval defined by the frequencies of the breathing modes of the two bubbles, repulsion of the two centres of mass is observed. Otherwise, the two bubbles always attract each other, and more effectively when $\omega_f = 0$. The domain where repulsion occurs is well characterized in the plane $\epsilon/D = 0$. Nevertheless, as ϵ/D or time increases its boundaries will be affected, since inertia will decrease the eigenfrequency of both breathing modes. The dependence of these frequencies on D may have an even more dramatic effect. For example, two bubbles with $D = 5$, $R = 0.7$ and $P_s = 666.66$ would attract each other if $\omega_f = 115$, since then $\omega_{0,l} \approx 74 < \omega_{0,r} \approx 110 < \omega_f = 115$ (Part 1). As they come closer together and provided they do not break up in the process, they may repel each other, since at $D = 2.5$ their eigenfrequencies would be $\omega_{0,l} \approx 72 < \omega_f = 115 < \omega_{0,r} \approx 120$. As they repel, the relative magnitude of the frequencies may change again and so on. Such effects are seen in figures 16, 17 and 20.

At this point it seems reasonable to re-evaluate our results in the context of relevant studies and compare the range of dimensionless quantities within which they occur. Spherical-cap shapes were originally observed in rising bubbles at high Reynolds numbers, Davies & Taylor (1950). Several common features of the accelerating motion studied here and that of rising bubbles motivate our belief that such shapes are produced by a similar mechanism. In particular, in the case of bubbles rising in low-viscosity fluids, $Re \geqslant 200$, a critical Weber number exists, $We \approx 1.2$, beyond which steadily rising and spherical bubbles are not observed, Hartunian & Sears (1957). The motion of their centre of mass becomes 'zig-zag' or spiral instead of rectilinear. The above investigators, as well as Saffman (1956), primarily attribute this transition to an instability 'triggered' by the interaction between surface tension and inertia forces in the direction of acceleration. Saffman also suggests that this instability, subsequently, initiates an oscillation of the wake of the bubble which establishes the oscillatory trajectory. At even larger Re and We the motion becomes rectilinear again and finally spherical-cap shapes appear with a very irregular and rapidly fluctuating shape on their lower surface; Saffman (1956) and Hartunian & Sears (1957).

In the present formulation three-dimensional disturbances are not allowed, hence zig-zag or spiral motions cannot be captured. However, spherical-cap shapes are observed with the side facing away from the direction of acceleration significantly deformed and oscillating on its own right, see also Part 1. They occur when the Bond number, based on the average acceleration, becomes larger than 1.5 when $P_s = 666.66$. As was pointed out before, this is also due to the domination of inertia over surface tension forces. Examination of table 5.7 in Pelekasis (1991) or figure 9 in Part 1 shows that when $D = 4$, $R = 1$, $P_s = 666.66$ and $\epsilon = 0.2$, then $Bo = \langle g \rangle = 1.8$ and spherical-cap shapes appear at $t \approx 1.0$. Considering that the average acceleration does not change significantly with time, a good estimate for the average dimensionless rectilinear velocity of a bubble is 2, when transition occurs. This value has been verified by direct calculations also. Given our definition of dimensionless quantities, the

dimensionless velocity coincides with the Weber number for the rectilinear motion of the bubbles. When the material properties of distilled water are used, the static pressure $P_s = 666.66$ gives a bubble radius of 1 mm and the value for the critical We obtained above corresponds to a linear velocity of 53.8 cm/s and to a critical Re of 1076.

These values should be compared with the ones given by Hartunian & Sears for the onset of instability in rising air bubbles in distilled water under atmospheric pressure. The critical values that they reported are $Re = 670$, $We = 1.22$ and a terminal velocity $u = 35.5$ cm/s for bubbles of radius 0.085 cm. Clearly, both instabilities occur within the same parameter range and are associated with the same type of force balance. The critical velocity is overpredicted here, which should be expected since it signals the appearance of spherical-cap shapes that occur for higher Re and We than the zig-zag or spiral motion. Furthermore, the extent of overprediction will be reduced when small viscous effects are included, in which case the rectilinear motion will be decelerated towards the late stages of motion. For very large values of Re and on a timescale $O(Re^{\frac{1}{2}})$, which is much greater than the timescale within which most of the effects presented here occur, $O(\epsilon^{-1})$, viscous forces will become large enough to balance inertia and induce a steady terminal velocity of both bubbles.

Another phenomenon related to the problem studied here is that of the erratic motion of bubbles often observed in cavitation experiments (Kornfeld & Suvorov 1944). The parametric excitation of shape oscillations in isolated bubbles was proposed by Benjamin & Strasberg (1958) as a cause of this type of motion. In their analysis Hall & Seminara (1980) argued that bubble translation might arise as a nonlinear effect following the growth of non-spherical modes, or through interaction of the bubble with an axisymmetric basic flow. According to the same analysis, however, bubble translation could arise at orders higher than the second, so that the growth rate of P_1, the mode associated with bubble translation, could increase from zero. In a recent study Benjamin & Ellis (1990) presented a more complete mechanism extending an idea first proposed by Saffman (1967). Namely, they assumed a form of the velocity potential and showed that a deformable bubble can propel itself in a perfect fluid as a result of nonlinear coupling of consecutive spherical Legendre modes (i.e. both n and $n+1$ modes must be initially present). Consequently, oscillating bubbles may be propelled along erratic paths as a result of multiple interactions between consecutive spherical harmonics, excited by an acoustic field through harmonic or subharmonic resonance. Furthermore, they argued that chaotic motion may also arise as a result of mode interactions with disturbances along the path of the bubble.

The present work shows how bubble interactions will induce and alter the translation and acceleration of a bubble and give rise to such a velocity potential. Moreover, it is shown that translation may be stronger than that merely attributed to mode coupling and that a variety of instabilities may arise leading to breakup or coalescence. All these effects have been reported by Kornfeld & Suvorov (1944), but they cannot be predicted by assuming a form of the velocity potential. Finally, in view of the large accelerations experienced by a bubble in the presence of a larger one, one can imagine that in a suspension of bubbles their interactions will have a very important effect on the intensity and direction of their motion.

This research was supported by the Fluid Mechanics Programme of the National Science Foundation under grant no. MSM-8705735 and the New York Science and Technology Foundation under grant no. SSF(88)-06. Usage of the Cornell National Supercomputer Facilities (CNSF) and the graphics software developed by Dr A. Poslinski are gratefully acknowledged.

REFERENCES

BENDER, C. M. & ORSZAG, S. A. 1978 *Advanced Mathematical Methods for Scientists and Engineers.* McGraw-Hill.

BENJAMIN, T. B. & ELLIS, T. A. 1990 Self-propulsion of asymmetrically vibrating bubbles. *J. Fluid Mech.* **212**, 65–80.

BENJAMIN, T. B. & STRASBERG, M. 1958 Excitation of oscillations in the shape of pulsating gas bubbles; Experimental work. *J. Acoust. Soc. Am.* **30**, 697.

BJERKNES, V. F. K. 1906 *Fields of force.* Columbia University Press.

BJERKNES, V. F. K. 1909 *Die Craftfelder.* Vieweg.

BLAKE, J. R. & CERONE, P. 1982 A note on the impulse due to a vapour bubble near a boundary. *J. Austral. Math. Soc.* B **23**, 383–393.

BLAKE, J. R. & GIBSON, D. C. 1981 Growth and collapse of a vapour cavity near a free surface. *J. Fluid Mech.* **111**, 123–140.

BLAKE, J. R., TAIB, B. B. & DOHERTY, G. 1986 Transient cavities near boundaries. Part 1. Rigid boundary. *J. Fluid Mech.* **170**, 479–497.

CRUM, L. A. 1974 Bjerknes forces on bubbles in a stationary sound field. *J. Acoust. Soc. Am.* **57**, 1363–1370.

CRUM, L. A. & NORDLING, D. A. 1972 Velocity of transient cavities in an acoustic stationary wave. *J. Acoust. Soc. Am.* **52**, 294–301.

DAVIES, R. M. & TAYLOR, G. I. 1950 The mechanics of large bubbles rising through extended liquids and through liquids in tubes. *Proc. R. Soc. Lond.* A **200**, 375–390.

ELLER, A. I. & CRUM, L. A. 1970 Instability of the motion of a pulsating bubble in a sound field. *J. Acoust. Soc. Am.* **47**, 762–767.

ESCHE, R. 1952 Untersuchung der Schwingungskavitation in Flüssigkeiten. *Acustica* **2**, 208–218.

FLYNN, H. G. 1964 *Physical Acoustics* (ed. W. P. Mason), vol. 1B, chap. 9, pp. 57–172. Academic.

HALL, P. & SEMINARA, G. 1980 Nonlinear oscillations of non-spherical cavitation bubbles in acoustic fields. *J. Fluid Mech.* **101**, 423–444.

HARTUNIAN, R. A. & SEARS, W. R. 1957 On the instability of small gas bubbles moving uniformly in various liquids. *J. Fluid Mech.* **3**, 27–47.

KORNFELD, M. & SUVOROV, L. 1944 On the destructive action of cavitation. *J. Appl. Phys.* **15**, 495–506.

LAMB, H. 1932 *Hydrodynamics*, 6th edn. Cambridge University Press.

LAUTERBORN, W. 1976 Numerical investigation of nonlinear oscillations of gas bubbles in liquids. *J. Acoust. Soc. Am.* **59**, 283–293.

LAUTERBORN, W. & CRAMER, E. 1981 Subharmonic route to chaos observed in acoustics. *Phys. Rev. Let.* **47**, 1445–1448.

NEPPIRAS, E. A. 1969 Subharmonic and other low-frequency emission from bubbles in sound-irradiated liquids. *J. Acoust. Soc. Am.* **46**, 587–601.

PELEKASIS, N. A. 1991 A study on drop and bubble dynamics via a hybrid boundary element-finite element methodology. PhD thesis, SUNY at Buffalo.

PELEKASIS, N. A. & TSAMOPOULOS, J. A. 1993 Bjerknes forces between two bubbles. Part 1. Response to a step change in pressure. *J. Fluid Mech.* **254**, 467–499.

PELEKASIS, N. A., TSAMOPOULOS, J. A. & MANOLIS, G. D. 1991 Nonlinear oscillations of liquid shells in zero gravity. *J. Fluid Mech.* **230**, 541–582.

PELEKASIS, N. A., TSAMOPOULOS, J. A. & MANOLIS, G. D. 1992 A hybrid finite-boundary element method for inviscid flows with free surface. *J. Comput. Phys.* **101**, 231–251.

PLESSET, M. S. & PROSPERETTI, A. 1977 Bubble dynamics and cavitation. *Ann. Rev. Fluid Mech.* **9**, 145–185.

SAFFMAN, P. G. 1956 On the rise of small air bubbles in water. *J. Fluid Mech.* **1**, 249–275.

SAFFMAN, P. G. 1967 The self-propulsion of a deformable body in a perfect fluid. *J. Fluid Mech.* **28**, 385–389.